# Optimal Sampling Conditions for Estimating Grassland Parameters via Reflectance Model Inversions

J. L. Privette, Ranga B. Myneni, W. J. Emery, *Member, IEEE,* and Forrest G. Hall

*Abstract*—The sensitivity of grassland bidirectional reflectance to soil, vegetation, irradiance, and sensor parameters is assessed. Based on these results, a vegetation Bidirectional Reflectance Distribution Function (BRDF) model is inverted with ground reflectance data from the First ISLSCP Field Experiment (FIFE). Results suggest that leaf area index (LAI) is most accurately retrieved from data gathered in near-infrared bands at low solar zenith angles (SZA), and leaf angle distribution is best retrieved from data gathered in near-infrared bands at high SZA. Generally, leaf optical properties are more accurately estimated from data acquired at high SZA. Canopy albedo and fraction of absorbed photosynthetically active radiation (fAPAR) are also estimated and compared to measured values. Albedo estimates are accurate to about ±0.01 (4% relative) when model parameters are determined from reflectance data gathered under preferred conditions. Estimates of fAPAR are less accurate. These results provide a guide for efficiently sampling surface reflectance and accurately retrieving parameters for use in climate and ecosystem models.

## I. INTRODUCTION

OPTICAL and structural properties of vegetation affect the transfer of energy, mass, momentum, and trace gases at the earth's surface. Process models (climate, biogeochemistry, ecosystem) therefore rely on accurate vegetation information for useful results. For example, global fields of rainfall, temperature and motion in General Circulation Models (GCM's) are affected by surface albedo [1]. Studies suggest this albedo must be accurate to within ±0.05 [2]. Similarly, photosynthetically active radiation absorbed (APAR) by vegetation is correlated with photosynthetic rates and plant growth in the absence of limiting stresses [3]. Photosynthetic rates determine the amount of carbon fixed by vegetation and hence affect the carbon cycle and primary production.

Satellite remote sensing techniques are often used to estimate surface parameters over large areas. Commonly, a vegetation index (VI) is employed. Indices (e.g., Normalized Difference Vegetation Index [NDVI]) have been correlated with many variables including leaf area index (LAI), biomass, fraction of APAR (fAPAR), vegetation conductance, potential evapotranspiration, and atmospheric carbon dioxide concentration. These relationships, however, can be site and sampling geometry dependent [4]–[6]. Although some indices [4], [7] are less sensitive to distorting factors, Myneni *et al.* [8] recently showed that most indices essentially detect pigment abundance per unit area. Thus, further relationships are indirect and subject to other influences.

A different technique for estimating surface parameters is the inversion of bidirectional reflectance (BRDF) models [9]. Physically-based models permit the simulation of all media affecting reflectance (soil, canopy, atmosphere) (e.g., [10]). Thus, they are applicable to all sites and sampling conditions. Their inversion allows the quantitative determination of parameters (e.g., LAI, leaf reflectance) that can be used directly by some process models (e.g., [11]). Moreover, reflectance models can be used to estimate surface state parameters such as albedo, APAR, and photosynthetic efficiency over diurnal cycles.

Nevertheless, inversions of bidirectional reflectance models with satellite data are not at an operational level. Thus, some issues requiring further study may be better addressed using simulated satellite data from ground-based instruments. This study builds on a previous investigation [12] which considered the preferred angular sample sets for determination of surface properties via model inversion. Specifically, ground-based reflectance data gathered over a tallgrass prairie during the First ISLSCP Field Experiment (FIFE) were used to estimate parameters of the soil and vegetation. The accuracy of retrieved values was assessed as a function of solar angle and spectral band. In addition, surface albedo and fAPAR are estimated and compared to *in situ* data.

## II. MODEL VALIDATION AND SENSITIVITY STUDY

### A. Model Introduction

DISORD is a numerical BRDF model based on the turbid medium approximation ([13], [14]). It accounts for all known scattering mechanisms and includes a hot spot formulation. The model depends primarily on measurable physical prop-

erties. Specifically, canopy depth is specified with the LAI parameter. The leaf angle distribution (LAD) is prescribed with the Beta distribution [15]. This distribution is a function of four parameters $(\mu(\theta), \nu(\theta), \mu(\varphi), \nu(\varphi))$ which may be determined analytically from leaf angle data. Diffuse leaf scattering is bi-Lambertian; its magnitude depends on leaf reflectance $(\rho)$ and transmittance $(\tau)$. Specular leaf reflectance depends on the refractive index $(\eta)$. The magnitude of the hot spot is determined by a parameter denoted HSP. Although DISORD can simulate reflectance from heterogeneous surfaces, a 1-D approximation (i.e., horizontal homogeneity) was used here.

The upper and lower boundary conditions in DISORD may both be anisotropic. Anisotropic soil reflectance is simulated with the model of Jacquemoud *et al.* [16]. This model is a function of six parameters, five of which may be considered spectrally invariant. Anisotropic diffuse irradiance may also be specified, although isotropic diffuse irradiance was assumed in this study. The latter parameterization depends only on the ratio $(\gamma)$ of direct-to-total irradiance.

The discrete ordinates method is used to solve the radiative transport equation. In this method, photon travel is restricted to a finite set of directions. These directions are chosen to be the ordinates of a quadrature scheme such that the angular integrals are evaluated accurately. All calculations in this study utilized six ordinates per octant for a total of 48 directions in the unit sphere. The spatial derivative is approximated by a finite difference scheme, resulting in a system of algebraic equations which can be solved by iteration on the scattering integral. Further details may be found elsewhere [11].

## B. Site Description

FIFE data were used throughout this study. FIFE included the coordinated measurement of soil, vegetation and atmospheric properties from ground, aircraft and satellite-based sensors [17]. The experiment was conducted on a 15 km × 15 km site near Manhattan, KS. Four Intensive Field Campaigns (IFC's; periods of more comprehensive measurements) were conducted in 1987, and an additional campaign (IFC-5) was conducted during July–August 1989.

Site 916, an area of concentrated sampling during IFC-5, was chosen for this study. This site was a relatively flat area of tallgrass prairie. The vegetation mainly included C4 grasses. The site was burned in the spring of 1989 to remove dead vegetation from previous years. Grazing did not occur. The soil was of the Dwight Series.

## C. Reflectance Data Description

Reflectance data from a Barnes Modular Multiband Radiometer (MMR) were collected by a team from the University of Nebraska [18]. The MMR has seven bands in the shortwave spectrum (0.45–0.52, 0.52–0.60, 0.63–0.69, 0.76–0.90, 1.15–1.30, 1.55–1.75, and 2.08–2.35 $\mu$m). It had a 15° instantaneous field of view (IFOV) and was mounted approximately 3.5 m off the ground. This resulted in a ground IFOV of about 0.75 m$^2$ at nadir.

A circle of six 3 m × 3 m plots was defined at site 916. Five of the plots were left intact and sampled for canopy reflectance.
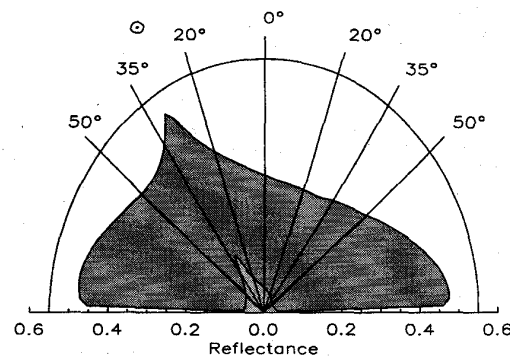


Fig. 1. Sampling geometry of the FIFE ground MMR instrument. The plane of the paper represents the principal plane, and the radial lines represent view zenith angles. The dark (light) shaded region depicts the band 4 NIR (band 3 red) reflectance as determined through forward modeling. Measured soil and canopy parameters (Table II) were used in the computation. The solar zenith angle was 30° (sun represented with circle).

TABLE I
NORMALIZED SPECIES ABUNDANCES USED TO DETERMINE CANOPY PARAMETERS AT SITE 916. SPECIES WITH LESS THAN 2% ABUNDANCE WERE DISREGARDED. ROWS WITHOUT DATA INDICATE SPECIES FOR WHICH MEASURED PROPERTY DATA WERE NOT AVAILABLE

| Species | Site Means | Leaf Optical Properties | Leaf Angles |
|---|---|---|---|
| Little bluestem | 0.240 | 0.331 | |
| Big bluestem | 0.222 | 0.306 | 0.493 |
| Indian grass | 0.157 | 0.216 | 0.349 |
| Purple love grass | 0.152 | | |
| Blue gramma | 0.051 | | |
| Switchgrass | 0.047 | 0.065 | 0.105 |
| Lead plant | 0.035 | 0.048 | |
| Inland ironweed | 0.024 | 0.033 | 0.054 |

The MMR sampled the plots at seven view zenith angles in the principal plane (Fig. 1). Typically, three samples were collected at each angle. In this study, all samples at a given angle were averaged. Only data gathered on August 4 and 8, 1989 (IFC-5), were used. Solar zenith angles (SZA's) ranged from 20 to 60° during the measurement periods. Rainfall did not occur during this period, and canopy parameters were assumed to remain constant.

The MMR boom and housing shadowed the target area at some sun-target-sensor geometries. Thus, all data were checked for shadow contamination based on trigonometric analysis. Data sets containing contaminated samples were eliminated from further analysis. This resulted in 23 complete data sets, each defined by seven samples per band at a given plot and SZA.

## D. Determination of Canopy Parameters

Measured canopy parameters were required throughout this study. As only LAI was measured for the actual mixed canopy, other parameters were estimated through an abundance-weighted averaging of species data.

Species abundances were measured in 15 plots at site 916. Species with less than 5% live green cover in a plot were not recorded. In the present study, mean plot abundances were summed and normalized. Species with normalized abundances <2% were disregarded. The remaining eight species and their abundances are given in Table I.

TABLE II

MEANS AND STANDARD DEVIATIONS OF SPECTRALLY-VARIANT PARAMETERS AT SITE 916 IN EARLY AUGUST 1989. SPECTRALLY-INVARIANT PARAMETER VALUES WERE $\{LAI, \mu(\theta), \nu(\theta)\} = \{1.94 \pm 0.61, 0.860 \pm 0.063, 2.244 \pm 0.368\}$ FOR VEGETATION AND $\{h, b, c, b', c'\} = \{1.098, 0.294, 0.093, 0.204, -0.030\}$ FOR THE SOIL [19]. STANDARD DEVIATIONS OF LAI AND $\omega_s$ WERE DETERMINED FROM SITE 916 DATA; REMAINING VALUES WERE DETERMINED FROM ALL AVAILABLE DATA. SINCE SOIL PARAMETERS WERE RETRIEVED VIA INVERSION, STANDARD DEVIATIONS ARE NOT AVAILABLE

| Band | $\rho$ | | $\tau$ | | $\omega_s$ | |
|---|---|---|---|---|---|---|
| | $\mu$ | $\sigma$ | $\mu$ | $\sigma$ | $\mu$ | $\sigma$ |
| 1 | 0.101 | 0.026 | 0.041 | 0.021 | 0.091 | 0.095 |
| 2 | 0.174 | 0.036 | 0.144 | 0.041 | 0.205 | 0.046 |
| 3 | 0.097 | 0.050 | 0.053 | 0.054 | 0.259 | 0.061 |
| 4 | 0.452 | 0.032 | 0.490 | 0.038 | 0.347 | 0.091 |
| 5 | 0.424 | 0.059 | 0.510 | 0.051 | 0.490 | 0.132 |
| 6 | 0.320 | 0.046 | 0.436 | 0.048 | 0.603 | 0.099 |
| 7 | 0.252 | 0.082 | 0.318 | 0.067 | 0.652 | 0.099 |

Of the eight species, leaf optical data were available for six species and LAD data were available for four. Abundance fractions were therefore summed and renormalized for both parameters (Table I). These fractions were used to weight the species data in the determination of canopy means. Species data obtained closest in time to August 4–8, 1989 (or during the same period of plant life) were used. Only green leaf data were used since dead leaf LAI $\ll$ green leaf LAI. The mean zenith LAD, determined from leaf angle measurements, was used to estimate the canopy Beta coefficients $(\mu(\theta), \nu(\theta))$. The HSP parameter was estimated based on previous studies [14].

Mean parameter values are reported in Table II. The LAI value is the mean value from five destructive samples. LAD results suggest the canopy was predominately erectophile with a mean tip angle of about 65°. Although azimuthal LAD data were collected, a uniform distribution was assumed here.

### E. Determination of Soil Parameters

Because a Lambertian soil approximation can cause significant errors in top-of-canopy (TOC) reflectance [19], an anisotropic background model [16] was used here. In a separate study [19], this model was inverted using soil reflectance data from site 916. The optimal set of retrieved parameter values $\{\omega_{s,1-7}, h, b, c, b', c'\}$ is given in Table II. These parameters include seven spectral values of the particulate single scattering albedo $(\omega_{s,1-7})$, a roughness parameter $(h)$, and four coefficients of the Legendre phase function expansion $(b, c, b', c')$. Excluding $\omega_s$, the retrieved values were applicable over all encountered solar angles, moisture levels and spectral bands. Errors in principal plane reflectance were generally less than 10%, although errors off the principal plane may be greater. Since the parameters were determined from bare soil data, their applicability to soils covered with canopy litter is not known.

### F. Determination of Irradiance Parameters

The ratio $(\gamma)$ of direct-to-total irradiance was not measured in the MMR bands during FIFE. Therefore, the 5S atmospheric model [20] was used. 5S was configured with water vapor, ozone, and the aerosol optical depth data collected during IFC-5. Values were updated for each MMR measurement period. The thermodynamic profile was determined from the US62 at-
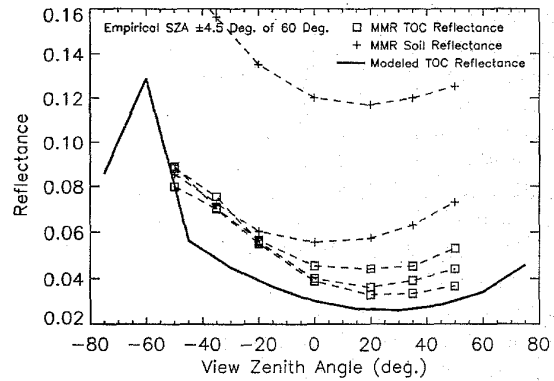


Fig. 2. Comparison of measured and modeled TOC reflectance in principal plane. Reflectances was determined for band 3 (red) at SZA = 60°. Measured parameter values (Table II) were used. Squares (□) represent TOC data and pluses (+) represent soil data. SZA of measured data were within ±4.5° of 60°.

mosphere, and a continental aerosol distribution was assumed. The MMR band sensitivities were assumed constant over the full wave half maximum (FWHM) wavelengths. Results showed that $\gamma$ increased with wavelength while its variance decreased [19]. This suggests that spectrally-independent surface parameters may be more accurately retrieved from data gathered at longer wavelengths.

### G. Model Validation

A partial validation of DISORD was accomplished by comparing modeled and measured reflectance values. Mean parameter values (Table II) were used together with mean atmospheric properties. Representative plots of red (band 3) and NIR (band 4) reflectance are shown in Figs. 2 and 3. Both TOC and soil reflectance data are shown. Although the model overestimated the red reflectance (errors <0.02 absolute), the differences may be due to soil effects. Specifically, the range of measured soil reflectance per angle is nearly twice the magnitude of the canopy reflectance. This large variability is probably due to moisture differences. A bright soil may substantially increase TOC reflectance, especially in canopies with many gaps. Since most turbid medium models do not account for gaps, model estimates may be lower than measured values. The NIR estimates (Fig. 3) are within the range of measured values for all view angles. Although the soil reflectance variability is similar to the red case in absolute units, it is lower relative to the canopy reflectance. Thus, its impact is reduced.

This test suggests that the estimates of model parameters were reasonable and that the model is able to simulate canopy reflectance with acceptable accuracy. The latter condition is imperative to the success of the inversion problem.

### H. Sensitivity Study

Mathematically, the number of retrievable parameters in an inversion is limited only by the number of data points. In practice, additional constraints are imposed due to inaccuracies in the model (e.g., turbid medium assumption, absence of
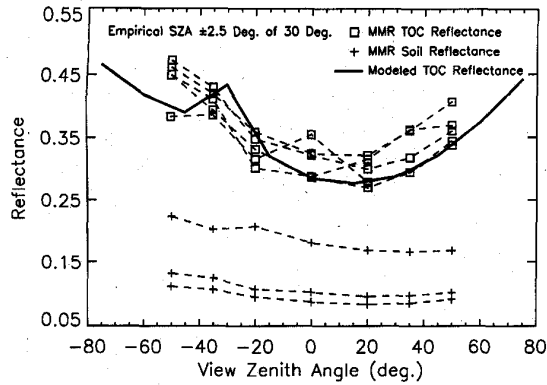
Fig. 3. Same as Fig. 2, but for band 4 (NIR) and SZA = 30°. The SZA of measured data were within ±2.5° of 30°.

nonleaf material), inefficiencies of optimization algorithms (e.g., trapping at nonglobal minima) and limitations of the data (e.g., noise, correlated samples). These drawbacks can lead to an overdetermination of the reflectance data and erroneous inversion solutions. Thus, a sensitivity study was performed to determine which parameters most affect canopy reflectance.

A "baseline" reflectance distribution was computed using the mean parameter set (Table II). The distribution was sampled in seven directions according to the FIFE MMR sampling scheme (see Fig. 1). Next, each model parameter was perturbed in turn by 10% of its range, positively and negatively. For each perturbation, a new reflectance distribution was computed. The rms difference between the baseline and perturbed reflectance distributions was determined. The sensitivity $(S)$ to the parameter was then recorded, where

$$S = \frac{\text{rms}}{\bar{r}_j^b} \cdot 100, \qquad (1)$$

and

$$\text{rms} = \sqrt{\frac{1}{7} \sum_{j=1}^{7} (r_j - \bar{r}_j^b)^2}, \qquad (2)$$

where $r_j^b$ is the baseline reflectance in direction $j$, $r_j$ is the geometrically-analogous reflectance of the perturbed distribution, and $\bar{r}_j^b$ is the mean of the seven baseline reflectance values. This process was repeated for three SZA's (30, 45, and 60°) and two MMR bands (red and NIR). Although $\gamma$ was determined from measured data (Section II-F), it was included here to assess the impact of errors in its estimation.

Sensitivity values are given in Table III. For both bands, results show TOC reflectance is most sensitive to leaf reflectance. This sensitivity increases notably with SZA in the red. Since leaves strongly absorb red photons, a higher SZA results in a much longer path optical depth. The increased path depth provides more opportunities for the canopy (versus the relatively bright soil) to affect the photon distribution. The distribution changes most in the backscatter region. At NIR wavelengths, lower leaf absorption results in a smaller change with increasing SZA. Sensitivity to leaf transmittance is nearly the same as for leaf reflectance in the NIR, however it is substantially less in the red. These results agree with

## TABLE III

SENSITIVITY $(S$, FROM (1)) OF TOC REFLECTANCE IN PRINCIPAL PLANE TO PARAMETER PERTURBATIONS. PERTURBATIONS EQUALED 10% OF THE THEORETICAL OR PRACTICAL RANGES. COLUMNS REPRESENT DIFFERENT SZA'S (30, 45, AND 60°) AT TWO WAVELENGTHS (RED AND NIR). THIN LINES SEPARATE ATMOSPHERIC, SOIL AND VEGETATION PARAMETERS, RESPECTIVELY. $\gamma$ IS THE DIRECT-TO-TOTAL IRRADIANCE RATIO, $h$ IS THE SOIL ROUGHNESS PARAMETER, $b$, $c$, $b'$, AND $c'$ ARE SOIL PHASE FUNCTION PARAMETERS, $\omega_s$ IS THE SOIL SINGLE SCATTERING ALBEDO, HSP IS THE CANOPY HOT SPOT PARAMETER, $\rho$ AND $\tau$ ARE LEAF REFLECTANCE AND TRANSMITTANCE, AND $\mu(\theta), \nu(\theta), \mu(\varphi)$, AND $\nu(\varphi)$ ARE COEFFICIENTS OF THE LAD. BASE CASE PARAMETER VALUES ARE GIVEN IN TABLE II

| Parameter | Red (Band 3) | | | NIR (Band 4) | | |
|---|---|---|---|---|---|---|
| | 30° | 45° | 60° | 30° | 45° | 60° |
| $\gamma$ | 6.95 | 6.66 | 5.92 | 1.80 | 2.36 | 3.02 |
| $h$ | 0.46 | 0.41 | 0.27 | 0.36 | 0.31 | 0.25 |
| $b$ | 8.68 | 6.08 | 2.50 | 3.41 | 2.49 | 1.59 |
| $c$ | 7.92 | 5.56 | 2.20 | 1.77 | 1.08 | 0.39 |
| $b'$ | 6.57 | 3.98 | 2.02 | 2.90 | 1.99 | 1.34 |
| $c'$ | 4.91 | 3.93 | 1.90 | 1.08 | 0.71 | 0.27 |
| $\omega_s$ | 14.86 | 10.66 | 5.15 | 6.42 | 5.19 | 3.82 |
| HSP | 2.73 | 3.08 | 1.17 | 1.00 | 1.11 | 0.42 |
| $\rho$ | 60.67 | 71.44 | 82.34 | 23.60 | 24.15 | 24.33 |
| $\tau$ | 19.12 | 28.78 | 46.57 | 18.68 | 19.86 | 21.38 |
| $\mu(\theta)$ | 4.62 | 4.09 | 5.26 | 10.10 | 7.74 | 7.18 |
| $\nu(\theta)$ | 1.87 | 2.45 | 3.33 | 3.81 | 2.57 | 2.32 |
| $\mu(\phi)$ | 0.75 | 0.93 | 2.66 | 2.14 | 2.41 | 2.87 |
| $\nu(\phi)$ | 1.74 | 1.01 | 2.88 | 4.27 | 4.02 | 4.33 |
| LAI | 22.54 | 22.11 | 18.08 | 20.72 | 20.16 | 18.09 |

[21]. The sensitivity to leaf transmittance at red increases significantly with SZA. The sensitivity increases most sharply at high SZA's due to changes in forward scattering. At NIR wavelengths, however, leaf albedo is relatively high such that there is significant multiple scattering. Thus, canopy forward scattering and reflectance sensitivity do not change as much with SZA.

Relative to the sensitivities to the leaf optical properties, the sensitivity to LAI is significantly lower at red than at NIR. Due to high leaf absorption, the canopy behaves optically semiinfinite at a lower LAI for red photons. As conditions become semiinfinite, reflectance becomes insensitive to perturbations in optical depth (LAI). Sensitivity to LAI decreases with increasing SZA since this also leads to longer path optical depths (more semiinfinite conditions). This result differs from that in [9], where sensitivity to LAI increased with SZA. The fourth most influential parameter at red is $\omega_s$, the impact of which decreases with increasing SZA. At NIR, $\mu(\theta)$ is fourth and $\omega_s$ is fifth. The relative brightness of the soil with respect to the canopy causes the differences in sensitivity order between the bands. The sensitivity to the remaining parameters is not significantly different for either band.

For model inversions, one set of adjustable parameters—influential over every band and solar angle combination—was desired. The model clearly is sensitive to the set $\{\rho, \tau, \text{LAI}, \omega_s\}$ in both bands. Although the model is rather sensitive to $\mu(\theta)$ at NIR, its sensitivity to $\mu(\theta)$ at red is less than its sensitivity to $b, c, b'$, and $c'$ for low SZA's. Nevertheless, $\mu(\theta)$ was kept variable and $b, c, b'$, and $c'$ were fixed. This decision followed from the sensitivity study and [19]. The latter suggested that $\{h, b, c, b', c'\}$ are essentially invariant with soil moisture and wavelength. Since LAD depends on two parameters ($\mu(\theta)$ and $\nu(\theta)$), both parameters were included in the adjustable set. Thus,

for inversion purposes, the set $\{LAI, \rho, \tau, \mu(\theta), \nu(\theta), \omega_s\}$ remained adjustable and the set $\{h, b, c, b', c', \mu(\phi), \nu(\phi)\}$ was fixed. Note the adjustable set contains parameters of both vegetation and soil.

## III. MODEL INVERSIONS

### A. Problem Configuration

The general inversion problem may be stated as follows: given a set of empirical directional reflectance data, determine the set of model parameters such that the computed directional reflectances best fit the empirical data. The fit of the empirical data is determined by a merit function [9], $\varepsilon^2$, defined here as

$$\varepsilon^2 = \sum_{j=1}^{n} \left( r_j - r_j^* \right)^2 \tag{3}$$

where $r_j$ is the directional reflectance for a given scan and solar angle geometry, $r_j^*$ is the geometrically-analogous model estimate, and $n$ is the number of reflectance samples. Although a variable weighting scheme may be introduced into (3), equal weighting was assumed here. The inversion of a DISORD prototype was systematically explored in [21].

Inversions were conducted individually for each of the seven spectral bands and 23 data sets. Thus, seven samples were used to determine six parameters. This configuration was used based on the redundancy in sampling (each sample represents an average of three measurements), the clarity of the atmosphere, and the high information content in principal plane reflectance [21].

Several measures were taken to help insure the global minimizer was found. First, (3) was minimized using a simplex routine (subroutine AMOEBA, [22]). This routine outperformed several other optimization routines in a separate study [21]. Second, broad parameter limits, based on theory and expected values, were imposed (e.g., $0 < LAI < 10$). Although the initial simplexes spanned the resulting parameter space, they were not necessarily the optimal choices. Third, the simplex routine was modified to permit variable expansion coefficients such that all vertex movements fell within the allowed parameter space. Fourth, minimization was terminated only after the merit function values (see (3)) of all vertices were to within $10^{-7}$. This value was found to be satisfactory in [21]. Finally, the procedure was restarted once after the initial convergence.

### B. Spectral Band and Solar Angle Analysis of Results

Below, inversion results for each parameter are discussed relative to the spectral band and SZA. To achieve greater statistical significance, SZA's were binned either above or below 40° (approximately the center of the range). Cases with a retrieved $LAI < 0.1$ were eliminated since this condition precludes a reasonable determination of any model parameter. The number of cases averaged per band/solar angle combination is given in Table IV. Note that reflectance data were obtained from five different plots and surface parameters were measured at additional plots. Because of

### TABLE IV

MEAN ERRORS (WITH MEAN RELATIVE ERRORS IN PARENTHESES) AND STANDARD DEVIATIONS IN RETRIEVED LEAF REFLECTANCE AS A FUNCTION OF BAND AND SZA. MEASURED VALUES ($\rho_o$) ARE ALSO SHOWN. THE NUMBERS OF SAMPLES USED TO GENERATE MEANS ARE SHOWN NEXT TO STANDARD DEVIATIONS

| Band | $\rho_o$ | SZA < 40° ME (MRE) | $\sigma$ | no. | SZA > 40° ME (MRE) | $\sigma$ | no. |
|---|---|---|---|---|---|---|---|
| 1 | 0.101 | 0.052 (51.5) | 0.020 | 13 | 0.022 (21.8) | 0.007 | 10 |
| 2 | 0.174 | 0.100 (57.5) | 0.049 | 10 | 0.027 (15.5) | 0.044 | 9 |
| 3 | 0.097 | 0.071 (73.2) | 0.031 | 13 | 0.053 (54.6) | 0.042 | 9 |
| 4 | 0.452 | 0.084 (18.6) | 0.079 | 13 | 0.002 (0.4) | 0.033 | 10 |
| 5 | 0.424 | 0.054 (12.7) | 0.061 | 13 | -0.015 (-3.5) | 0.031 | 10 |
| 6 | 0.320 | 0.138 (43.1) | 0.125 | 10 | -0.006 (-1.9) | 0.066 | 10 |
| 7 | 0.252 | -0.115 (-45.6) | 0.043 | 13 | -0.113 (-44.8) | 0.019 | 10 |

surface heterogeneity, some variability is to be expected in the results in Table IV [32].

Results are indicated as mean errors (ME) and mean relative errors (MRE, in %), where

$$ME = \frac{1}{n} \sum_{i=1}^{n} (P_i - P_0), \tag{4}$$

and

$$MRE = \frac{1}{n} \sum_{i=1}^{n} \frac{(P_i - P_0)}{P_0} \cdot 100, \tag{5}$$

where $P_0$ is the measured parameter value, $P_i$ is the retrieved parameter value for data set $i$, and where $n$ is the number of data sets.

Estimates of leaf reflectance were most accurate at high SZA's (Table IV). Standard deviations were generally lower at high SZA as well. These results are consistent with [21] and the sensitivity analysis which showed increasing model sensitivity to leaf reflectance with increasing SZA (Table III). Because a high SZA results in less photon interaction with the soil, errors introduced by incorrectly retrieved/estimated soil parameters are reduced. Leaf reflectance errors were lowest (<0.006, 1.9%) in the NIR (bands 4 and 6). The superiority of NIR bands may be due to the greater magnitude of canopy reflectance relative to soil reflectance. This increases the effective signal-to-noise ratio.

Leaf transmittance, in contrast, was most accurately estimated at high SZA's for visible bands, but at low SZA's for NIR bands (Table V). These trends are predictable given the spectra of soil and vegetation. When the background is bright relative to the canopy (as in the visible), less photon interaction with the background (larger canopy path length) is preferable. The high sensitivity of canopy forward scattering to leaf transmissivity leads to better results at high SZA. When the canopy is much brighter than the background (NIR), results are best if the background receives greater irradiance (low SZA). This probably occurs since changes in TOC reflectance due to changes in the soil contribution—as determined by leaf transmittance at low SZA—exceed those due to changes in canopy forward scattering at high SZA. These trends also follow previous results [21]. Standard deviations were generally lower for all bands at high SZA's.

Although errors in the soil single scattering albedo (Table VI) were not well correlated with SZA, a comparison of modeled soil reflectance using retrieved $\omega_s$ is revealing (Fig. 4). The modeled soil spectrum followed the measured

### TABLE V

MEAN ERRORS (WITH MEAN RELATIVE ERRORS IN PARENTHESES) AND STANDARD DEVIATIONS IN RETRIEVED LEAF TRANSMITTANCE AS A FUNCTION OF BAND AND SZA. MEASURED VALUES ($\tau_o$) ARE ALSO SHOWN

| Band | $\tau_o$ | SZA < 40° ME (MRE) | $\sigma$ | SZA > 40° ME (MRE) | $\sigma$ |
|---|---|---|---|---|---|
| 1 | 0.041 | -0.015 (-36.6) | 0.037 | 0.009 (21.9) | 0.012 |
| 2 | 0.144 | -0.028 (-19.4) | 0.061 | -0.018 (12.5) | 0.031 |
| 3 | 0.053 | -0.013 (-24.5) | 0.067 | 0.012 (22.6) | 0.023 |
| 4 | 0.490 | -0.026 (-5.3) | 0.078 | -0.047 (-9.6) | 0.042 |
| 5 | 0.510 | 0.010 (1.9) | 0.057 | -0.015 (-2.9) | 0.056 |
| 6 | 0.436 | 0.041 (9.4) | 0.054 | 0.060 (13.7) | 0.061 |
| 7 | 0.318 | -0.021 (-6.6) | 0.130 | -0.114 (35.8) | 0.036 |

### TABLE VI

MEAN ERRORS (WITH MEAN RELATIVE ERRORS IN PARENTHESES) AND STANDARD DEVIATIONS IN RETRIEVED SOIL SINGLE SCATTERING ALBEDO AS A FUNCTION OF BAND AND SZA. MEASURED VALUES ($\omega_{so}$) ARE ALSO SHOWN

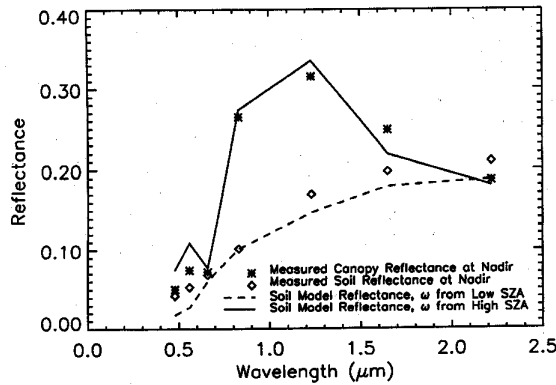| Band | $\omega_{so}$ | SZA < 40° ME (MRE) | $\sigma$ | SZA > 40° ME (MRE) | $\sigma$ |
|---|---|---|---|---|---|
| 1 | 0.091 | -0.043 (-47.3) | 0.038 | 0.111 (122.0) | 0.053 |
| 2 | 0.205 | -0.129 (-62.9) | 0.050 | 0.084 (41.0) | 0.104 |
| 3 | 0.259 | -0.098 (-37.8) | 0.017 | -0.050 (-19.3) | 0.078 |
| 4 | 0.347 | -0.084 (-24.2) | 0.091 | 0.262 (75.5) | 0.130 |
| 5 | 0.490 | -0.124 (-25.3) | 0.036 | 0.206 (42.0) | 0.127 |
| 6 | 0.603 | -0.170 (-28.2) | 0.039 | -0.086 (-14.3) | 0.124 |
| 7 | 0.652 | -0.202 (-31.0) | 0.138 | -0.208 (-31.9) | 0.045 |



Fig. 4. Nadir reflectance from the soil model using mean $\omega_s$ retrieved from canopy model inversions. Diamonds ($\diamond$) represent soil reflectance as measured by MMR at nadir, and asterisks ($*$) represent equivalent TOC reflectance. Solid line shows soil model reflectance for $\omega_s$ retrieved at high SZA. Dashed line shows the equivalent for $\omega_s$ retrieved at low SZA.
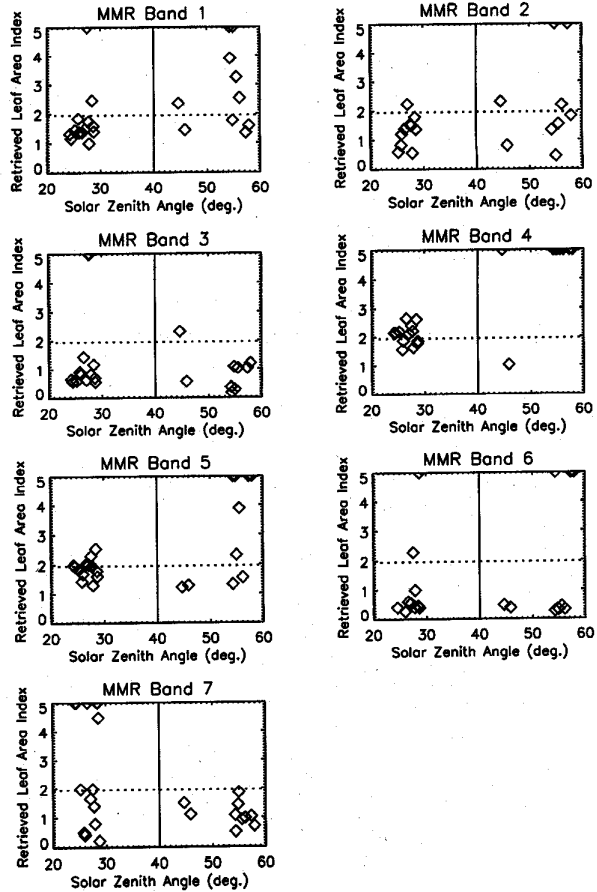


Fig. 5. Retrieved LAI as a function of spectral band (ordered sequentially from left to right, top to bottom) and SZA. Horizontal dotted line indicates mean measured LAI. Vertical line partitions SZA bins. The accuracy and consistency of inversions with NIR bands (4 and 5) at low SZA is apparent. For graphing purposes, values greater than 5.0 were set equal to 5.0.

soil spectrum for $\omega_s$ retrieved at low SZA's, but followed the measured vegetation spectrum for $\omega_s$ retrieved at high SZA's. Also, standard deviations in errors were lower at low SZA. However, the inversion underestimated $\omega_s$ in all bands for low SZA's. The overestimation of leaf reflectance (Table IV) probably led to this systematic deviation. Recall also the "measured" $\omega_s$ values were not directly measured, but were estimated via inversions [19]. Moreover, there were undoubtedly differences in soil moisture and canopy litter between the bare soil and vegetated plots. Still, the relatively low sensitivity of DISORD (Table III) to all soil parameters underscores the difficulty in retrieving soil properties from TOC reflectance data.

Results for LAI are shown in Fig. 5 and Table VII. Means and standard deviations of the errors generally increase with SZA. This is consistent with the sensitivity analysis which

### TABLE VII

MEAN ERRORS (WITH MEAN RELATIVE ERRORS IN PARENTHESES) AND STANDARD DEVIATIONS IN RETRIEVED LAI AS A FUNCTION OF BAND AND SZA. THE MEASURED LAI VALUE WAS 1.94 ± 0.61

| Band | SZA < 40° ME (MRE) | $\sigma$ | SZA > 40° ME (MRE) | $\sigma$ |
|---|---|---|---|---|
| 1 | 0.225 (11.6) | 2.382 | 1.006 (51.9) | 1.632 |
| 2 | -0.641 (-33.0) | 0.524 | 0.466 (24.0) | 1.914 |
| 3 | 0.044 (2.3) | 2.894 | -1.045 (-53.9) | 0.658 |
| 4 | 0.157 (8.1) | 0.347 | 5.103 (263.0) | 2.587 |
| 5 | -0.068 (-3.5) | 0.331 | 2.484 (128.0) | 3.547 |
| 6 | -0.590 (-30.4) | 2.110 | 1.027 (52.9) | 4.266 |
| 7 | 1.845 (95.1) | 3.759 | -0.828 (-42.7) | 0.395 |

shows the sensitivity of TOC reflectance to LAI decreases with increasing SZA (path optical depth). However, it is contrary to results found in [9], [12], and [21]. The best LAI estimates were provided by bands 4 and 5 (NIR) at low SZA's, where the mean errors were less than 0.16 (8.1%) and the standard deviations were less than 0.35 (see Fig. 5, bands 4 and 5). This error is well within the uncertainty of the measured value. The spectral band preference also follows from the sensitivity study, since the sensitivity to LAI at NIR exceeded the sensitivity to LAI at red, relative to other parameters.
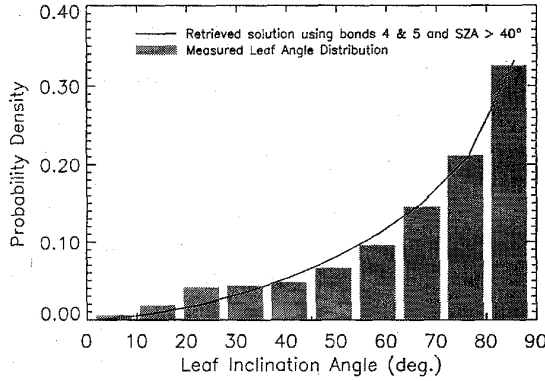
Fig. 6. Comparison of the mean measured LAD (bars) with retrieved Beta LAD (line). The retrieved distribution was determined by averaging results from NIR bands and high solar zenith angles (Section III-B). Retrieved distribution was determined at bin centers and normalized.

To determine the most accurate estimation of LAD, the $\chi^2$ statistic was employed [22],

$$\chi^2 = \sum_{j=1}^{10} \frac{\left(f_j - f_j^*\right)^2}{f_j + f_j^*}, \tag{6}$$

where $f_j^*$ is the retrieved fraction of leaf normals in zenith angle bin $j$, and $f_j$ is the measured fraction. The retrieved fractions were determined at the bin centers and normalized. The retrieved distribution is closest to the measured distribution when $\chi^2$ is lowest. The mean estimates of $\mu(\theta)$ and $\nu(\theta)$, their standard deviations and the associated $\chi^2$ values are given in Table VIII. The closest approximations were achieved in NIR bands 4 and 5 at high SZA's ($\chi^2 = 0.037$ and 0.008, respectively). This agrees with [12]. The average LAD from these two bands ($\chi^2 = 0.020$) matches the true distribution well (Fig. 6). The preference of NIR bands for the estimation of the LAD is obvious from the sensitivity study results (Table III). Relative to leaf optical properties, the sensitivity to LAD parameters is greater at NIR wavelengths. The lack of a strong dependence on SZA in the NIR inversion results is also consistent with the sensitivity study. The greater dependence on SZA in results for other bands is more consistent with the sensitivity results for the red band. This may be due to the increased reflectance anisotropy at high SZA.

### C. Surface Albedo

Although the MMR bands are not contiguous over the shortwave frequencies, surface albedo may be estimated using the "extended band" method of Starks et al. [23]. In this method, the MMR bandwidths are artificially extended such that all shortwave frequencies are represented (Table IX). The fraction $\left(\bar{W}_i\right)$ of shortwave energy incident in each band is used to weight the broad-band spectral albedo $\left(\overline{ALB}_i\right)$. The total albedo (ALB) is estimated by summing the spectral products

$$ALB = \int_{0.3}^{4.0} ALB_\lambda W_\lambda d\lambda = \sum_{i=1}^{7} \overline{ALB}_i \bar{W}_i, \tag{7}$$

TABLE VIII
MEAN ERRORS AND STANDARD DEVIATIONS IN RETRIEVED LAD
PARAMETERS $(\mu(\theta), \nu(\theta))$ AS A FUNCTION OF SPECTRAL BAND AND
SZA. ERRORS IN LAD ARE CHARACTERIZED BY $\chi^2$: LOWER VALUES
INDICATE FITS CLOSER TO THE MEASURED DISTRIBUTION. THE MEASURED
VALUES WERE $\{\mu(\theta), \nu(\theta)\} = \{0.860 \pm 0.063, 2.244 \pm 0.368\}$

SZA < 40°

| Band | $\mu(\theta)$ ME | $\sigma$ | $\nu(\theta)$ ME | $\sigma$ | $\chi^2$ |
|---|---|---|---|---|---|
| 1 | 1.183 | 0.678 | 2.554 | 0.265 | 0.228 |
| 2 | 0.752 | 0.995 | 1.801 | 1.292 | 0.135 |
| 3 | 0.604 | 0.864 | 1.907 | 1.335 | 0.100 |
| 4 | 0.119 | 0.708 | 0.964 | 1.452 | 0.038 |
| 5 | 0.345 | 0.397 | 1.261 | 1.404 | 0.061 |
| 6 | 0.623 | 1.621 | 2.451 | 0.572 | 0.102 |
| 7 | 2.366 | 2.125 | 2.293 | 0.707 | 0.562 |

(a)

SZA > 40°

| Band | $\mu(\theta)$ ME | $\sigma$ | $\nu(\theta)$ ME | $\sigma$ | $\chi^2$ |
|---|---|---|---|---|---|
| 1 | 0.373 | 0.395 | 2.115 | 0.450 | 0.076 |
| 2 | -0.190 | 0.392 | 1.724 | 1.520 | 0.116 |
| 3 | 0.212 | 0.838 | 2.298 | 0.891 | 0.085 |
| 4 | -0.014 | 0.310 | 0.924 | 1.323 | 0.037 |
| 5 | -0.189 | 0.162 | -0.100 | 0.939 | 0.008 |
| 6 | -0.180 | 0.214 | 1.426 | 1.583 | 0.091 |
| 7 | 0.782 | 1.411 | 1.806 | 1.858 | 0.143 |

(b)

TABLE IX
EXTENDED BANDWIDTHS USED TO COMPUTE ALBEDO VALUES. MEAN WEIGHTS
$(\bar{W}_i)$ AND STANDARD DEVIATIONS WERE DETERMINED FROM 5S RESULTS

| Band | Bandpass Limits | Extended Limits | $\overline{W}_i$ | $\sigma$ |
|---|---|---|---|---|
| 1 | 0.450-0.520 | 0.300-0.520 | 0.239 | 0.005 |
| 2 | 0.520-0.600 | 0.520-0.615 | 0.146 | 0.002 |
| 3 | 0.630-0.690 | 0.615-0.725 | 0.144 | 0.001 |
| 4 | 0.760-0.900 | 0.725-1.000 | 0.222 | 0.002 |
| 5 | 1.150-1.300 | 1.000-1.360 | 0.139 | 0.002 |
| 6 | 1.550-1.750 | 1.360-1.800 | 0.067 | 0.001 |
| 7 | 2.080-2.350 | 1.800-4.000 | 0.043 | 0.001 |

where

$$\bar{W}_i = \left[ \frac{\int_{\lambda_{a,i}}^{\lambda_{b,i}} I_{0,\lambda} d\lambda}{\int_{0.3}^{4.0} \lambda_{0,\lambda} d\lambda} \right], \tag{8}$$

and where $I_{0,\lambda}$ is the irradiance at $\lambda$, and $\lambda_{a,i}$ and $\lambda_{b,i}$ are the lower and upper limits of extended band $i$, respectively. Irradiance was determined with the 5S model. Average weights $(\bar{W}_i)$ and their standard deviations are given in Table IX. In DISORD, spectral albedo is determined through quadrature integration of the reflectance distribution. A previous study [21] suggested errors in spectral albedo may remain small despite significant errors in retrieved parameters.

In the cases below, albedo estimates from (7) were compared with mean measured values. The latter were determined from two pairs of pyranometers at site 916. The mean absolute error (MAE) and the mean of the relative absolute errors (MRAE) were calculated using (4) and (5), where $(P_i - P_0)$ was replaced with $|ALB_i^* - ALB_i|$ and where $ALB_i$ is the mean measured albedo and $ALB_i^*$ is the estimated albedo for data set $i$.

*1) Case 1:* Initially, $\overline{ALB}_i$ was calculated separately with the retrieved parameter set for each spectral band and solar angle combination. Thus, spectral albedo was determined
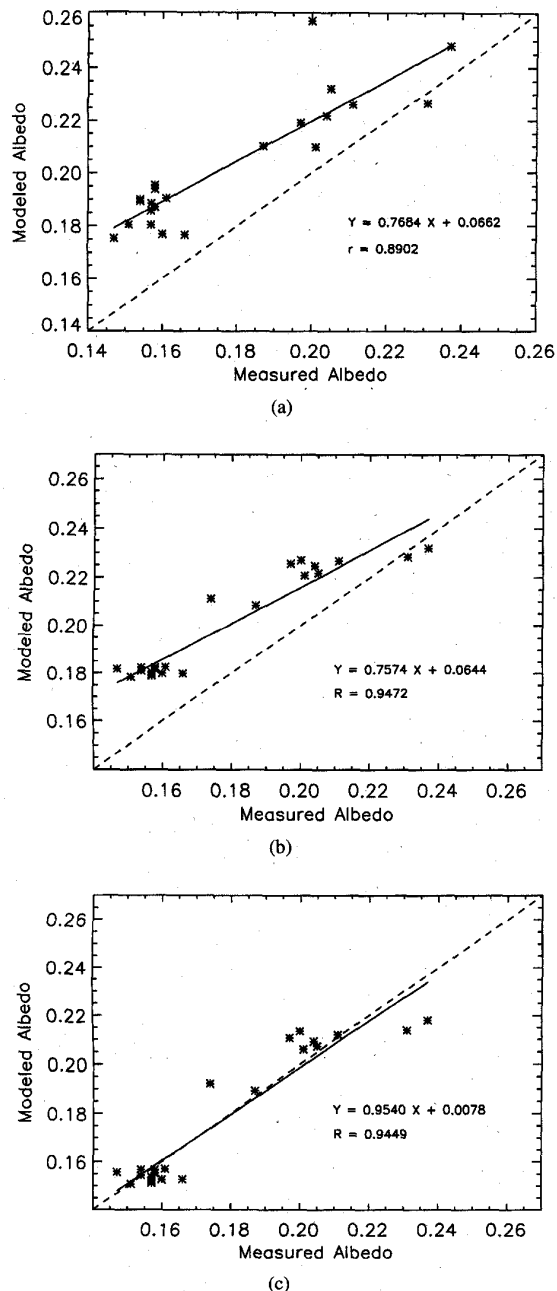
Fig. 7. Comparison of measured and modeled albedo. The dashed line is the 1-to-1 line. (a) Parameter sets were retrieved for each band and data set individually. This follows the method of Starks et al. [23]. (b) Parameter sets were determined from measured values (Table II). Only atmospheric properties and solar zenith angles were changed between model calculations. (c) Same as (b), but canopy parameters were determined from retrieved data at optimal wavelengths and solar zenith angles.

from seven reflectance samples. Albedo estimates exceeded the measured values in most cases (Fig. 7(a)). Differences decreased with increasing albedo. The MAE was 0.025, the MRAE was 14.9%, and the correlation coefficient $(r)$ was 0.89. Errors were not well correlated with either solar angle or $\gamma$.

Starks et al. [23] reported larger errors (MRAF = 22.4% for 1987 and 27.6% for 1988) using an empirical model and a

more diverse set of FIFE MMR data. The lower MRAE value in the present study may be due to the use of a physically-realistic model. Model accuracy is especially significant in directions for which data were not available during inversion. A notable systematic error, which caused the offset of the regression line in Fig. 7(a), was obvious in [23] as well. Sources of errors are comprehensively discussed in [23].

*2) Case 2:* In most process models, a single set of BRDF parameters must allow accurate calculations of albedo over a range of illumination conditions. To test the potential of a single parameter set, the measured parameter values (Table II) were used in DISORD to determine $\overline{ALB}_i$. A comparison of estimated and measured albedo is shown in Fig. 7(b). The MAE was 0.022 (MRAE = 13.0%)—a small improvement over Case 1. Again, errors decreased as albedo increased. Compared to Case 1, the regression coefficient improved notably $(r = 0.95)$. This suggests that random errors in Case 1 evolved from differences in inversion solutions.

*3) Case 3:* Based on the above results, a single set of retrieved parameters was used to estimate albedo. "Optimal" parameter values were determined based on spectral band and solar angle analysis (Section III-B). Specifically, leaf reflectance was obtained from results at high SZA (Table IV). Leaf transmittance in visible channels was obtained from results for high SZA's, while NIR transmittance was obtained from results for low SZA's (Table V). Soil ws was determined from results at low SZA's (Table VI). The LAI (1.985) was obtained by averaging results from bands 4 and 5 at low SZA's (Table VII). Finally, the LAD parameters $(\mu(\theta) = 0.7582, \nu(\theta) = 2.656)$ were found by averaging results from bands 4 and 5 at high SZA's (Table VIII). Albedo estimates are shown in Fig. 7(c). Compared to Case 2, the MAE (0.007; MRAE = 3.63%) was more than 10 times lower. This indicates a significant reduction in the systematic bias. The correlation $(r = 0.94)$ was similar.

Based on these results, two additional observations deserve comment. First, albedo results determined with variable parameter sets (Case 1) were less accurate than those found with a single parameter set (Cases 2 and 3). This suggests that solutions determined from limited data sets (e.g., seven principal plane samples at one SZA) may provide poor reflectance estimates in directions where data were absent during inversion. This leads to erroneous albedo estimates. Using preferred wavelengths and solar angles for parameter retrieval (Section III-B) seems to prevent this problem. Second, albedo results with retrieved canopy parameters were superior to those with measured parameters. This underscores the potential for determining "energy" variables (e.g., albedo) from energy data (e.g., angular reflectance). Essentially, inverse methods may compensate for errors in the BRDF model and parameter measurements. Errors in either can lead to poor results despite accuracy in the other.

### D. Fraction of Absorbed Photosynthetically Active Radiation (fAPAR)

Studies suggest that fAPAR has a near-linear relationship with some vegetation indices [24]. However, effects of viewing

TABLE X
EXTENDED BANDWIDTHS USED TO COMPUTE fAPAR AND $\text{fAPAR}_{\text{total}}$. MEAN
WEIGHTS ($\bar{W}_i$) WERE COMPUTED BY THE 5S MODEL. ALSO SHOWN ARE THE
NORMALIZED WEIGHTS AFTER CONVERSION FROM ENERGY UNITS TO
QUANTUM UNITS. STANDARD DEVIATIONS WERE NEGLIGIBLE IN EACH CASE

| Band | Bandpass Limits | Extended Limits | $\bar{W}_i$ [energy] | $\bar{W}_i$ [photons] |
|---|---|---|---|---|
| 1 | 0.450-0.520 | 0.400-0.520 | 0.410 | 0.345 |
| 2 | 0.520-0.600 | 0.520-0.615 | 0.330 | 0.342 |
| 3 | 0.630-0.690 | 0.615-0.700 | 0.261 | 0.313 |

geometry [18], canopy structure [25] and soil/background [25], [26] have hampered efforts to find a general VI-fAPAR relationship for the FIFE area. A recent study [21] suggested that absorbed radiation could be accurately estimated via BRDF model inversions. Below, this method is used to estimate fAPAR.

Algebraically, fAPAR is defined as

$$\text{fAPAR} = \frac{I_0 - R_c - (T_c - R_s)}{I_0}, \qquad (9)$$

where $I_0$ is the incident photon flux density (PFD), $R_c$ is the exitant PFD above the canopy, $T_c$ is the PFD transmitted through the canopy, and $R_s$ is the PFD reflected by the soil/background. PFD is defined as the number of photons (0.4–0.7 $\mu$m) incident per unit time on a unit surface $(\text{mol} \cdot \text{m}^{-2} \cdot \text{s}^{-1})$. Photon counts rather than energy units are used since photosynthetic rates are essentially independent of the energies of the absorbed photons [27]. Equation (9) can be approximated by letting $R_s = T_c R_c I_0^{-1}$ [18]. This effectively assumes the soil and TOC albedos are equal. With this substitution, fAPAR can be estimated with three sensors, as used in FIFE, instead of four.

For modeling purposes, fAPAR is defined similarly to albedo (see (7)),

$$\text{fAPAR} = \int_{0.4}^{0.7} F_{a,\lambda} W_\lambda d\lambda = \sum_{i=1}^{3} \bar{F}_{a,i} \bar{W}_i, \qquad (10)$$

where $F_{a,\lambda}$ is the fraction of radiant energy absorbed by the canopy at wavelength $\lambda$, and $\bar{F}_{a,i}$ is the mean fraction of radiant energy absorbed by the canopy in band $i$. All other variables are as defined above, except the integral limits in (8) are now 0.4 and 0.7 $\mu$m. DISORD directly evaluates $\bar{F}_{a,i}$ using quadrature integration and (9). Extended band limits and weights (determined from 5S) are shown in Table X. The standard deviations of the band weights were negligible.

Since 5S determines irradiance in $W$ m$^{-2}$, a correction based on Planck's Law $(K_\lambda \propto \lambda)$ was used to convert $W$ to mols$^{-1}$. The neglect of this correction biases the weights toward shorter wavelength (higher energy) bands (see Table X). To facilitate the use of standard 5S output, $\bar{W}_i$ in photon counts was approximated as

$$\bar{W}_i = \left[ \frac{\int_{\lambda_{a,i}}^{\lambda_{b,i}} I_{0,\lambda} d\lambda \, \bar{\lambda}_i}{\sum_{j=1}^{3} \bar{I}_0} \right] \qquad (11)$$

$$\bar{I}_0 = \int_{\lambda_{a,j}}^{\lambda_{b,j}} I_{0,\lambda} d\lambda \, \bar{\lambda}_j, \qquad (12)$$

where $\bar{\lambda}_i$ is the center wavelength of extended band $i$.

*1) Canopy fAPAR:* The fAPAR data were measured with a line quantum sensor during eight periods over the two days. The SZA range was 22 to 56°. Typically, five measurements were made within each period. Equation (10) was used to estimate fAPAR with both measured and retrieved model parameters. Atmospheric data collected near the time of the fAPAR measurements were used to estimate $\bar{W}_i$. The MAE and MRAE were calculated using (4) and (5), where $(P_i - P_0)$ was replaced with $|\text{fAPAR}_i^* - \text{fAPAR}_i|$, and where $\text{fAPAR}_i$ is the mean measured value and $\text{fAPAR}_i^*$ is the estimated value for data set $i$, and $n = 8$.

Modeled fAPAR values, determined with measured parameters (Table II), are plotted against mean fAPAR data in Fig. 8(a). Results show the modeled fAPAR consistently exceeded the measured values. The MAE was 0.174 (37.14% relative). The correlation coefficient was 0.906, which suggests the largest errors were systematic. The predominance of systematic errors and decreasing errors with increasing fAPAR (and SZA) are the same trends observed for the Case 2 albedo (measured parameters).

Second, the optimal canopy parameters—described in the Case 3 albedo study—were used (Fig. 8(b)). Since MMR data were not collected simultaneously with fAPAR, only data acquired closest in time to fAPAR acquisition periods were used. Again, the modeled values exceeded the measured values. However, the MAE was reduced by nearly 20% to 0.142 (MRAE $=$ 30.17%). The correlation coefficient (0.899) was similar to the case above. As in the albedo study, the model was more accurate when optimal retrieved parameters were used. In addition, errors decreased with increasing fAPAR (SZA). The lack of simultaneity in the MMR and fAPAR data acquisitions undoubtedly contributed to some of the differences.

*2) Total fAPAR:* To help isolate the sources of the fAPAR errors, total (canopy and soil) fAPAR values were also computed. Empirical $\text{fAPAR}_{\text{total}}$ values were determined by

$$\text{fAPAR}_{\text{total}} = I_0 - R_c. \qquad (13)$$

In DISORD,

$$\text{fAPAR}_{\text{total}} = \text{fAPAR} + \text{fASOIL} = 1.0 - \text{ALB}_{\text{PAR}}, \qquad (14)$$

where fASOIL is the fraction of PAR radiation absorbed by the soil. Thus, $\text{fAPAR}_{\text{total}}$ was determined by replacing $\bar{F}_{a,i}$ in (15) with $\overline{\text{ALB}}_i$, and subtracting the result from 1.0 (see (14)). Again, both the measured and the optimal retrieved parameters were used (Fig. 9(a) and (b), respectively). MAE and MRAE were determined as in the fAPAR calculation, except fAPAR was replaced with $\text{fAPAR}_{\text{total}}$.

Errors in $\text{fAPAR}_{\text{total}}$ were minimal. Estimates were within 0.04 (measured parameters) and 0.09 (retrieved parameters) of the measured values. The measured parameter set resulted in an MAE of 0.002 (MRAE $=$ 0.185%), while the optimal retrieved parameters produced an MAE of 0.005 (MRAE $=$ 0.503%). The correlation coefficients were 0.942 and 0.946, respectively. Unlike for albedo and fAPAR, errors in $\text{fAPAR}_{\text{total}}$ were larger when the retrieved parameters were used. Note that
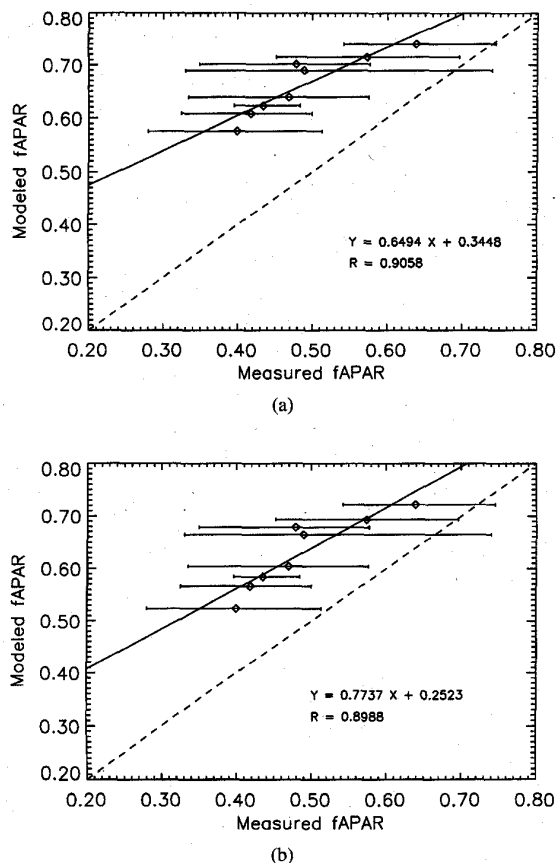
Fig. 8. Comparison of measured and modeled fAPAR. Error bars represent the minimum and maximum values per measurement period. Note that fAPAR was not measured simultaneously with MMR reflectance. The dashed line is the 1-to-1 line. (a) Canopy parameters were determined from measured values (Table II). Only atmospheric properties and solar zenith angles were changed between model calculations. (b) Same as (a), but canopy parameters were determined from retrieved data at optimal wavelengths and solar zenith angles.

Fig. 9. Comparison of measured and modeled $fAPAR_{total}$. Note that $fAPAR_{total}$ was not measured simultaneously with MMR reflectance. The dashed line is the 1-to-1 line. (a) Canopy parameters were determined from measured values (Table II). Only atmospheric properties and solar zenith angles were changed between model calculations. (b) Same as (a), but canopy parameters were determined from retrieved data at optimal wavelengths and solar zenith angles.

although fAPAR varied significantly over the eight periods, $fAPAR_{total}$ was relatively invariant (cf. Figs. 8(a) and (b) and 9(a) and (b)).

*3) Error Analysis:* As errors in fAPAR significantly exceeded those in $fAPAR_{total}$, some analysis of fAPAR error sources is warranted. First, errors in the band extension method were estimated using directional reflectance data gathered with a Spectron Engineering SE590 Spectroradiometer. Reflectance data were provided at every 5 nm of the PAR spectrum for canopy, litter, and soil. The canopy and soil data were obtained at site 916 during IFC-5, however the litter data were obtained at various sites on September 15, 1993 [31]. Only litter data obtained over previously burned sites were used. Data at the maximum view zenith angle (50° backscatter) were used to reduce contributions from underlying media.

Mean relative errors (MRE) were determined using (5), where $P_i$ was replaced with the mean SE590 reflectance over the MMR bandwidth, and $P_0$ was replaced with the mean SE590 reflectance over the extended bandwidth (Table X) for each data set. MRE values for each band and the PAR spectrum (using quanta weights from Table X) are shown
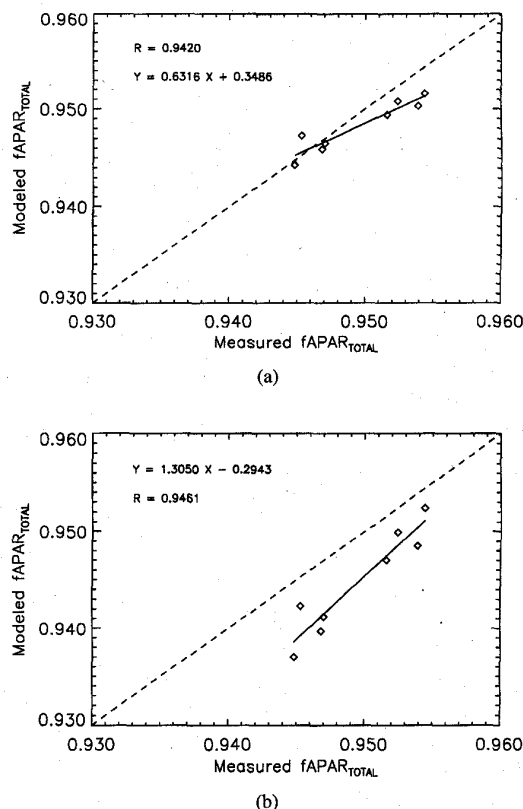
in Table XI. Errors were greatest in band 1, however the weighted PAR errors were below 3.3% for each component. The PAR reflectance error for the total soil, litter, and canopy system was 2.53% ($\sigma = 0.36\%$) as determined from nadir reflectance data. Note that MMR spectral sensitivity and bidirectional effects were largely ignored. For estimation of errors in *absorbed* radiation, optically semiinfinite media must be assumed (i.e., albedo must be considered the compliment of the absorbed fraction). The relatively small errors in Table XI were expected since the actual MMR bands cover about 70% of the PAR spectrum. This is considerably more than the 26% coverage of the shortwave spectrum (0.3–4.0 $\mu$m), for which the band extension method provided reasonable albedo estimates (Section III-C).

Second, if fAPAR is significantly overestimated and $fAPAR_{total}$ is reasonable, (14) requires that fASOIL be significantly underestimated—i.e., the modeled soil must be considerably brighter than the true soil. SE590 data suggests the litter was darker than the soil. Since litter was present below the canopy, estimates of $\omega_s$ based on bare soil reflectance would lead to an overestimation of actual background reflectance. However, estimates of $\omega_s$ determined through DISORD inversions with TOC data should have been

TABLE XI
MEAN RELATIVE ERRORS IN EXTENDED BAND REFLECTANCE DUE TO THE
ASSUMPTION OF CONSTANT REFLECTANCE OUTSIDE MMR BANDWIDTHS. TO
REDUCE EFFECTS FROM OTHER COMPONENTS, THE MAXIMUM VZA
(50° IN BACKSCATTER) WAS USED. RESULTS WERE AVERAGED OVER
MULTIPLE SZA'S. REFLECTANCE ERRORS OVER THE FULL PAR SPECTRUM
WERE DETERMINED USING THE QUANTUM BAND WEIGHTS IN TABLE X

| Component | MRE (%) | | | |
|---|---|---|---|---|
| | Band 1 | Band 2 | Band 3 | Weighted PAR |
| Canopy | 15.2 | 2.51 | -10.7 | 2.75 |
| Litter (Thatch) | 12.4 | -1.72 | -1.41 | 3.27 |
| Soil | 9.3 | -2.03 | 0.12 | 2.55 |

reasonable. Thus, errors in Figs. 8(b) and 9(b) should have been lower than those in Figs. 8(a) and 9(a). This did occur to some degree. Soil moisture differences may have had a similar effect. Finally, a previous study [19] suggests the soil model probably overestimated reflectance off the principal plane. Note the decrease in fAPAR errors with increasing SZA (increasing fAPAR) is as would be expected for a soil error source.

The last source of differences between modeled and measured fAPAR is the "measured" fAPAR. Three points are noteworthy. First, canopy heterogeneity at site 916 may have resulted in differences between MMR and fAPAR measurement plots [32]. Second, high variance in the fAPAR data (see error bars in Fig. 8(a) and (b)) was primarily due to large variability in transmitted flux measurements. Sources of this variability include instrument problems, canopy gaps and heterogeneity. Third, the approximation of (9) assumed that the TOC albedo equaled the soil albedo. If the true soil albedo exceeded the TOC albedo, this approximation would lead to underestimation of the actual fAPAR. Although soil albedo was not measured, soil reflectance exceeded TOC reflectance in some bands and directions.

### E. Other Sources of Errors

Although error sources have been identified in the sections above, several general error sources for inversion studies deserve review. First, there presently is not a method to insure global minimization in multiple variable problems, although several steps were taken in this study to insure optimality. Second, the MMR data were measured with a 15° IFOV instrument, yet the model assumes a unit steradian IFOV. This effect is more important in visible wavelengths where the angular reflectance varies more in proportion to the mean. Third, the MMR view angles were accurate to ±2° zenith and ±10° azimuth. This probably had minimal effect since samples near the hot spot (where reflectance changes are greatest) were filtered out. Fourth, isotropic diffuse irradiance was assumed throughout this study. Although this assumption is incorrect, its impact is not known and will be considered in future work. Finally, turbid medium models are not ideally suited to low LAI conditions. Still, for grassland applications, turbid medium models are probably the most reasonable.

### IV. CONCLUSION

A turbid medium reflectance model [13] can adequately simulate the top-of-canopy (TOC) reflectance of grasslands. The TOC reflectance is most sensitive to leaf optical properties. Sensitivity to leaf optical properties increases substantially as the solar zenith angle (SZA) increases. The third most influential parameter is LAI, the sensitivity to which decreases as SZA increases. LAI is nearly as influential as leaf optical properties in the NIR band, however it is substantially less influential in the red band. A leaf angle distribution (LAD) parameter and soil single scattering albedo $(\omega_s)$ are fourth and fifth most influential, not necessarily respectively. The TOC sensitivity to other parameters varies for different spectral bands.

The optimal spectral bands and solar angles for gathering data to estimate parameters were determined via model inversion. LAI is most accurately retrieved from NIR data gathered at low SZA. The mean LAI error ($\sim$0.1) is well within the accuracy suggested for agronomical and climatological needs [28]. The LAD is best retrieved from NIR data acquired at high SZA, although the dependence on SZA is not large. Leaf reflectance is most accurately retrieved from data gathered at high SZA, while leaf transmittance trends vary with spectral band. Mean errors in leaf optical properties below 0.03 are generally possible for preferred SZA conditions. Soil single scattering albedo is most reliably retrieved from data collected at low SZA. These results imply that LAI and ws may be difficult to retrieve for high latitude locations since low SZA conditions may not be possible.

Albedo was also estimated using both measured and retrieved model parameters. Results are most accurate when the "optimal" retrieved parameters, determined from data acquired at preferred wavelengths and SZA noted above, are used. Estimates accurate to ±0.01 (4% relative) are possible over a range of illumination angles. Superior results with retrieved parameter values, compared to measured values, suggest that estimating albedo from related radiation data (i.e., directional reflectance) is less subject to model and measurement errors. Errors appear to be larger when retrieved parameters are not obtained from data collected under preferred conditions. In these cases, more angularly diverse data may be needed to accurately estimate spectral albedo in some bands and SZA.

Estimates of fAPAR (canopy absorption) and fAPAR$_{total}$ (soil and canopy) were also determined. The model appears to overestimate fAPAR when either measured or retrieved parameters are used (37.14% and 30.17%, respectively). Errors decrease as SZA increases, however. Estimates of fAPAR$_{total}$ are accurate for all SZA. Although not quantified, the largest errors in fAPAR were probably due to differences in the conditions between the MMR and fAPAR measurement sites. This is particularly important for the soil model, since its parameters were determined from the reflectance of bare soil. Canopy litter was undoubtedly present below the actual canopy. Moreover, estimates of soil reflectance were probably erroneous for directions off the principal plane [19]. Finally, although the model accurately predicted TOC reflectance, it does not simulate canopy gaps. This may have led to its overestimation of fAPAR. It is anticipated that fAPAR estimation via inverse methods will improve with additional studies.

Although principal plane samples are most useful for inversion applications [21], the ability to scan nine samples in/near the principal azimuthal plane will routinely be possible upon launch of the EOS MISR instrument [29]. Other sensors, such as AVHRR and the EOS MODIS [30], also provide angularly diverse data. This study suggests that accurate determination of surface parameters, including albedo and fAPAR, from these sensors is (will be) possible.

## ACKNOWLEDGMENT

## REFERENCES

[1] J. Shukla and Y. Mintz, "Influence of land-surface evapotranspiration on the earth's climate," *Science*, vol. 215, pp. 1498–1500, 1982.
[2] A. Henderson-Sellers and M. F. Wilson, "Surface albedo data for climatic modeling," *Rev. Geophys. Space Phys.*, vol. 21, pp. 1743–1778, 1983.
[3] J. L. Monteith, "Solar radiation and productivity in tropical ecosystems," *J. Appl. Ecol.*, vol. 9, pp. 747–766, 1972.
[4] F. Baret and G. Guyot, "Potentials and limits of vegetation indices for LAI and APAR assessment," *Remote Sensing Environ.*, vol. 35, pp. 161–173, 1991.
[5] S. N. Goward and K. F. Huemmrich, "Vegetation canopy PAR absorptance and the normalized difference vegetation index: An assessment using the SAIL model," *Remote Sensing Environ.*, vol. 39, pp. 119–140, 1992.
[6] B. Pinty, C. Leprieur, and M. M. Verstraete, "Toward a quantitative interpretation of vegetation indices. Part 1: biophysical canopy properties and classical indices," *Remote Sensing Rev.*, vol. 7, pp. 127–150, 1993.
[7] B. Pinty and M. M. Verstraete, "GEMI: a nonlinear index to monitor global vegetation from satellites," *Vegetatio*, vol. 101, pp. 15–20, 1992.
[8] R. B. Myneni, F. G. Hall, P. J. Sellers, and A. L. Marshak, "Interpretation of spectral vegetation indexes," *IEEE Trans. Geosci. Remote Sensing* vol. 33, pp. 481–486, 1995.
[9] N. S. Goel and D. E. Strebel, "Inversion of vegetation canopy reflectance models for estimating agronomic variables I: problem definition and initial results using the Suits' model," *Remote Sensing Environ.* vol. 13, pp. 487–507, 1983.
[10] R. B. Myneni, G. Asrar, and F. G. Hall, "A three dimensional radiative transfer model for optical remote sensing of vegetated land surfaces," *Remote Sensing Environ.*, vol. 41, pp. 85–103, 1992.
[11] P. J. Sellers, Y. Mintz, Y. C. Sud, and A. Dalcher, "A simple biosphere model (SiB) for use within general circulation models," *J. Atmos. Sci.* vol. 43, pp. 505–531, 1986.
[12] N. S. Goel and R. L. Thompson, "Optimal solar/viewing geometry for an accurate estimation of leaf area index and leaf angle distribution from bidirectional canopy reflectance data," *Int. J. Remote Sensing*, vol. 6, pp. 1493–1520, 1985.
[13] R. B. Myneni, V. P. Gutschick, G. Asrar, and E. T. Kanemasu, "Photon transport in vegetation canopies with anisotropic scattering. Parts I through IV," *Agric. For. Meteorol.*, vol. 42, pp. 1–40 and 87–120, 1988.
[14] R. D. Stewart, "Modeling radiant energy transfer in vegetation canopies," Master's thesis, Kansas State Univ., Manhattan, 1990.

[15] N. S. Goel and D. E. Strebel, "Simple beta distribution representation of leaf orientation in vegetation canopies," *Agron. J.*, vol. 76, pp. 800–803, 1984.
[16] S. Jacquemoud, F. Baret, and J. F. Hanocq, "Modeling spectral and bidirectional soil reflectance," *Remote Sensing Environ.*, vol. 41, pp. 123–132, 1992.
[17] P. J. Sellers, F. G. Hall, G. Asrar, D. E. Strebel, and R. E. Murphy, "The first ISLSCP field experiment (FIFE)," *Bull. Amer. Met. Soc.*, vol. 69, pp. 22–27, 1988.
[18] E. A. Walter-Shea, B. L. Blad, C. J. Hays, M. A. Mesarch, D. W. Deering, and E. M. Middleton, "Biophysical properties affecting vegetative canopy reflectance and absorbed photosynthetically active radiation at the FIFE site," *J. Geophys. Res.*, vol. 97, pp. 18925–18934, 1992.
[19] J. L. Privette, R. B. Myneni, W. J. Emery, and B. Pinty, "Inversion of a soil reflectance model for use in vegetation BRDF models," *J. Geophys. Res.*, vol. 100, no. D12, pp. 25497–25508, 1995.
[20] D. Tanré, C. Deroo, P. Duhaut, M. Herman, J. J. Morcrette, J. Perbos, and P. Y. Deschamps, "Description of a computer code to simulate the satellite signal in the solar spectrum: The 5S code," *Int. J. Remote Sensing*, vol. 11, pp. 659–668, 1990.
[21] J. L. Privette, R. B. Myneni, C. J. Tucker, and W. J. Emery, "Invertibility of a 1-D discrete ordinates canopy reflectance model," *Remote Sensing Environ.*, vol. 48, pp. 89–105, 1994.
[22] W. H. Press, B. P. Flannery, S. A. Teukolsky, and W. T. Vetterling, *Numerical Recipes*. New York: Cambridge Univ. Press, 1986.
[23] P. J. Starks, J. M. Norman, B. L. Blad, E. A. Walter-Shea, and C. L. Walthall, "Estimation of shortwave hemispherical reflectance (albedo) from bidirectionally reflected radiance data," *Remote Sensing Environ.*, vol. 38, pp. 123–134, 1991.
[24] G. Asrar, R. B. Myneni, Y. Li, and E. T. Kanemasu, "Measuring and modeling spectral characteristics of a tallgrass prairie," *Remote Sensing Environ.*, vol. 27, pp. 143–155, 1989.
[25] T. H. Demetriades-Shah, E. T. Kanemasu, I. D. Flitcroft, and H. Su, "Comparison of ground- and satellite-based measurements of the fraction of photosynthetically active radiation intercepted by tallgrass prairie," *J. Geophys. Res.*, vol. 97, pp. 18947–18950, 1992.
[26] F. G. Hall, K. F. Huemmrich, S. J. Goetz, P. J. Sellers, and J. E. Nickeson, "Satellite remote sensing of surface energy balance: success, failures, and unresolved issues in FIFE," *J. Geophys. Res.*, vol. 97, pp. 19061–19090, 1992.
[27] R. W. Pearcy, "Radiation and light measurements," in *Plant Physiological Ecology, Field Methods and Instrumentation*, R. W. Pearcy, J. Ehleringer, H. A. Mooney, and P. W. Rundel, Eds. New York: Chapman and Hall, 1989, pp. 97–116.
[28] J. G. P. W. Clevers and W. Verhoef, "LAI estimation by means of the WDVI: A sensitivity analysis with a combined PROSPECT-SAIL model," *Remote Sensing Rev.*, vol. 7, pp. 43–64, 1993.
[29] D. J. Diner, C. J. Bruegge, J. V. Martonchik, T. P. Ackerman, R. Davies, S. A. W. Gerstl, H. R. Gordon, P. J. Sellers, J. Clark, J. A. Daniels, E. D. Danielson, V. G. Duval, K. P. Klaasen, G. W. Lilienthal, D. I. Nakamoto, R. J. Pagano, and T. H. Reilly, "A multi-angle imaging spectroradiometer for geophysical and climatological research from EOS," *IEEE Trans. Geosci. Remote Sensing*, vol. 27, pp. 200–214, 1989.
[30] V. V. Salomonson and D. L. Toll, "The moderate resolution imaging spectrometer-nadir (MODIS-N) facility instrument," *Adv. Space Res.* vol. 11, pp. 231–236, 1991.
[31] E. Walter-Shea, personal communication, 1994.
[32] D. Schimel, personal communication, 1994.
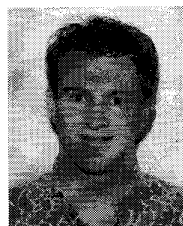
**J. L. Privette** earned the Ph.D. degree in aerospace engineering sciences from the University of Colorado, Boulder, in 1994.

He has been involved in remote sensing since 1989, primarily in the development and inversion of bidirectional reflectance models. He has been a Visiting Scientist at the National Center for Atmospheric Research and Université Blaise Pascal, France. He recently began work at NASA-Goddard Space Flight Center as an employee of the University of Maryland. His interests include the development of remote sensing products and their assimilation into ecosystem and climate models.

**Ranga B. Myneni** received the Ph.D. degree in biology from the University of Antwerp, Antwerp, Belgium, in 1985.

He was previously employed by Kansas State University, Mahattan, and Georg-August University in Goettingen, Germany, prior to joining Goddard Space Flight Center as an employee of the University of Maryland, College Park. His research interests are radiation transport and remote sensing of vegetation.
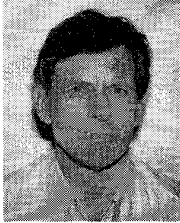
**W. J. Emery** (M'90) received the Ph.D. degree in physical oceanography from the University of Hawaii in 1975.

After working at Texas A&M University, College Station, he moved to the University of British Columbia, Canada, in 1978, where he created a Satellite Oceanography facility and program. He was appointed Full Professor in Aerospace Engineering Sciences at the University of Colorado, Boulder, in 1987 where he is the Director of the Center for Remote Sensing and Image Processing (CRSP). He is active in the analysis of satellite data for oceanography, meteorology, and terrestrial vegetation. In addition, his group writes analysis software and establishes/operates data systems for the distribution of satellite data received by their own antennas. He is a coauthor of two textbooks on physical oceanography, has translated two oceanographic books (German to English) and has authored over ninety refereed publications.

Dr. Emery is a member of the Laboratory for Atmospheric and Space Physics (LASP), the Program in Oceanic and Atmospheric Sciences (PAOS) and is on the CU Global Change Advisory Committee. He is a member of a number of NRC, NASA, and NOAA committees and panels including the EOSDIS Science Advisory Panel (known as the Data Panel). He is also co-chairman of the JPL and GSFC DAAC's User Working Groups. He is a member of the NASA Science User Network (NSUN) Committee.

**Forrest G. Hall** received the undergraduate degree in mechanical engineering from the University of Texas and the M.S. and Ph.D. degrees in physics from the University of Houston, Houston, TX.

He is with the NASA Goddard Space Flight Center's Laboratory for Terrestrial Physics where he currently serves as Research Scientist and Co-Project Manager for the Boreal Ecosystem-Atmosphere Study (BOREAS).